PREPRINT — DO NOT DISTRIBUTE

Mapping Greenland's Mass Loss in Space and Time

Christopher Harig,[1*] Frederik J. Simons[1]

[1]Department of Geosciences, Princeton University,
Guyot Hall, Princeton, NJ 08544, USA

[*]To whom correspondence should be addressed; E-mail: charig@princeton.edu.

Estimates of the mass lost from the Greenland ice sheet from data collected by the Gravity Recovery And Climate Experiment (GRACE) have widely varied (*1–3*). While the continentally and decadally averaged estimated trends have now more or less converged (*4, 5*), to this date there is little clarity on the precise spatial pattern of Greenland's mass loss, nor on how the geographical pattern has varied on relatively short time scales. Here we present a spatially and temporally resolved estimation of the ice mass change over Greenland between April 2002 and August 2011. While the total mass loss trend has remained steady, actively changing areas of mass loss were concentrated on the southeastern and northwestern coasts, with ice mass in the center of Greenland steadily increasing.

The contribution to global sea level rise from the melting of polar ice sheets has been a focus of intense study over the past several decades. Earth's second largest ice sheet, Greenland, has been surveyed by a multitude of techniques. Remote-sensing observations of laser and radar altimetry and InSAR have constrained both the overall variability in Greenland's mass

balance over time (*6–12*), and the local mass flux of its peripheral western and eastern outlet glaciers (*13–16*). These measurements have shown both strong variations among seasons and strong decadal variations in mass change rates (*11, 17*).

Coincident with these observations since 2002, the Gravity Recovery And Climate Experiment (GRACE) satellite mission has been mapping the Earth's geopotential field continuously, and many studies have used monthly snapshots of the geopotential field to estimate the Greenland's total yearly mass change (*1–3, 18–20*). These estimates have varied from -100 to -250 Gt/yr, although, as additional data have been added, the range has narrowed to close to -220 Gt/yr (*4,5*). One study (*20*) has reported accelerations in the annual mass loss of Greenland of about -30 Gt/yr^2.

The estimates of the spatial pattern of mass loss that can be made from GRACE are much less well constrained than those from remote sensing. Whereas remote-sensing techniques sample discrete areas on the surface, the geopotential measurement made by GRACE at altitude effectively samples over a broad region several hundred kilometers in diameter. In addition, due to the character of the errors in the data, it is commonly deemed necessary to employ spatial smoothing which further reduces the spatial resolution (*21*). GRACE results from the first half of the 2000s have shown broad mass loss along the eastern half of Greenland (*1–3*). Later work has shown that mass loss increased along the northwest coast of Greenland later in the decade (*4, 5, 19, 22*).

In this paper we determine the spatial distribution of mass loss over time with unprecedented detail compared to previous work, thanks to a new method of working with GRACE data products. Using spherical Slepian functions (*23*) we use more of the signal contained within the noisy GRACE data, and are able to resolve the spatial changes in mass loss on a yearly basis. We thereby settle the controversies surrounding the geographical pattern of Greenland's ice loss, and the presence or absence of significant accelerations in the ongoing trends.

Spherical harmonics are an orthogonal basis for the sphere, making the distribution of "Stokes" expansion coefficients the method of choice for the release of the GRACE Level-2 data products. These are currently bandlimited, complete to degree and order 60. When we wish to examine only a region, e.g. Greenland, spherical harmonics are no longer ideal as they lack orthogonality over the region. Estimating a regional signal this way thus becomes quite a complex operation and the results have an unfavorable error structure (*24*), which makes significance testing and detailed interpretation all but impossible. To deal with these difficulties, some authors have chosen to give up spatial resolution altogether by using averaging functions over the landmass to determine the broad total rate of mass change over time (*3*,*25*). Others have expanded the GRACE coefficients into the space domain to estimate trends on a latitude-longitude grid combined with forward modeling of mass anomalies (*1*, *4*). Still others parameterize either the direct intersatellite range measurements (*2*) or the global Level-2 solutions (*5*) into basin-scale local mass variations. All of these methods make assumptions about the data or the models that limit their spatial sensitivity, either by using predefined basin shapes, using basis functions that are not orthogonal, performing smoothing or post-processing to reduce assumed errors but thereby potentially reducing the signal itself, or by outright spatial averaging. We postulate that the historical lack of agreement between GRACE-based models of Greenland's mass loss is at least partly due to the failure to fully characterize the trade-offs and uncertainties that accompany these various choices of averaging, filtering and parameterization that have been made. Indeed, these dwarf the uncertainties on elastic structure of the substrate or the magnitude of post-glacial rebound corrections, both of which are needed to convert mass anomalies to estimates of ice mass lost due to melting.

We thus bypass the commonly used filtering and averaging procedures altogether, and use a simple method, with only a few assumptions of a statistical and computational nature that have been tested through extensive simulation. We base our estimation on an analysis in the

spherical Slepian basis. The Slepian basis, which is formed by optimization (*23*), constitutes a fully orthogonal bandlimited basis for a region of interest, in our case Greenland, and allows us to obtain a spatial sensitivity that is superior to that of the non-optimal methods. Using only those functions that have the majority of their energy concentrated within the region of interest dramatically improves the signal-to-noise ratio, and the results experience very little influence from signal originating outside the region of interest; minimization of the well-known leakage problem is indeed the explicit optimization objective in the construction of the Slepian basis (*26*).

We used 108 monthly GRACE Release-4 geopotential fields from the Center for Space Research, University of Texas at Austin, covering the time span from April 2002 to August 2011 (including five gap months). The highly variable degree-two order-zero spherical-harmonic coefficient is replaced with values from satellite laser ranging, as is by now customary (*27*). The GRACE geopotential data are transformed into surface mass density using the classical method of Wahr *et al.* (*28*). The surface mass density is subsequently projected onto a Slepian basis designed to capture the region within Greenland's coastlines but including a small buffer zone of 0.5°. The bandwidth of the Slepian basis, $L = 60$, matches the bandwidth of the GRACE data products. We truncate the expansion at the effective dimension of the combined spatio-spectral space (Greenland in space, bandlimited spectrally), known as the Shannon number (*23*). This leaves only twenty target functions, each of which are "eigenmaps" that have their energy highly concentrated over Greenland. This sparse model space represents a significant reduction of the original spherical-harmonic dimension, which comprised $(L+1)^2 = 3721$ functions whose expansion coefficients are substantially influenced by noise and required estimating by the alternative methods. As described, our method involved only the selection of the size of the buffer zone, the choice of bandwidth, and the number of terms in the Slepian expansion (see the

Supplementary Online Material). The rationale behind our selections is validated by extensive simulation.

The post-glacial rebound model of Paulson *et al.* (*29*), is similarly projected into this basis and subtracted from the data. The total mass over the region, relative to a nine-year mean (Fig. 1), is then calculated by integrating each function over the region, scaling by its corresponding expansion coefficient, and summing over the twenty functions. We estimate measurement error by fitting a linear trend, and a function with a period of one year to each of the Slepian coefficient time series, and generating a covariance matrix from the residuals. This gives a conservative measure of the variance of each coefficient, which we extend to the uncertainty of their sum via linear error propagation.

The total mass change (Fig. 1) shows a clear trend as well as an annual variation. We calculate the best-fitting linear trend covering all 108 months and find the mass change rate over our whole region to be -219.9$\pm$7.9 Gt/yr. The two-sigma uncertainty on the trend derives from the fit covariance matrix, and does not include the uncertainty in the post-glacial rebound correction (*30*). Fitting an additional quadratic term (see the Supplementary Online Material), we find the acceleration of mass loss to be a modest -8.3$\pm$3.9 Gt/yr^2. In Fig. 1, the error envelope for the fit is shown with dashed lines. The overall trend is very well determined, since with almost a decade of data the fit covers many seasonal cycles, which can vary strongly between years. On this subject our results are in agreement with the most recent studies, but in obtaining it we have relied on far fewer processing steps by the judicious choice of basis, as described above. A reestimation of the trends up to the year 2006, in which three studies appeared with much variability in the conclusions (*1–3*), reconciles the estimates as nearly falling within each other's uncertainties when evaluated according to our method. We conclude that the discrepancies in the literature were more a matter of statistics rather than physics or data selection.

Using an extension of our approach to estimate the average mass trend we are able to measure the spatial pattern of mass change and how it changes with time. To each of our twenty Slepian-function expansion-coefficient time series we have fit either a 1st, 2nd, or 3rd order polynomial, depending on whether each additional term passed an F-test for significance. This then becomes our new estimate for the signal. These fits embody the gradual changes over time spans of several years, and ignore much of the variability within each year. Fig. 2 displays a map of the total mass change of the estimated signal over the eight-year period from January 2003 to January 2011 (*31*). There is a clear concentration of mass loss along the coasts, mainly in the southeast and in the northwest, where radar interferometry reports large ice flow speeds associated with outlet glaciers (*9*). While the broad-scale agreement with prior results from GRACE (*22*) is a tribute to the quality and longevity of the data, the degree of spatial localization that we derive from the Slepian-basis methodology significantly shrinks the geographical footprint that can now be robustly modeled.

In the central high-elevation portions of Greenland there is evidence for significant accumulation of ice mass, much more clearly so than seen in previous GRACE studies (*4, 19, 22*). Accumulation in the interior of Greenland is an expected result of a warming climate (*8*) and has been observed with studies of satellite altimetry (*6, 9, 10, 32*). Our observation of the interior mass accumluation is spatially very well resolved and this, too, represents a significant improvement over earlier attempts to localize this anticipated pattern from GRACE data alone.

The better-resolved spatial maps of Greenland's mass loss are accompanied by the possibility to extract higher-resolution temporal variations of the geographic signal. When each year is examined in more detail (Fig. 3) the loci of largest mass loss move around Greenland with time. In 2003 and 2004, mass loss is concentrated along the entire eastern coast of Greenland. In 2005 and 2006, mass loss was reduced in the northeast while it increased in the southeast. Meanwhile, mass loss began to increase along the northwest coast. From 2007 to 2010, mass

loss further increased in northwest Greenland while mass loss diminished in the southeast coast areas after 2008. Each year has a region in the interior of Greenland with mass increase of > 5 cm/yr (light blue), and that region has shifted slightly from year to year.

Overall, these spatially shifting mass changes match well to remote-sensing observations. The increased mass loss in southeast Greenland first seen in 2005 coincides with accelerated flow observed in eastern outlet glaciers during that time (*15*). Increasing mass losses in northwest Greenland since 2006 are also seen in observations of radar interferometry and GPS (*11*,*22*). The observed deceleration in mass loss in the southeast in 2009 and 2010 may be related to decreased glacier velocities in that region (*33*) although continued study is needed to substantiate this claim.

Our results together demonstrate both the power of spatiospectrally concentrated "Slepian" localization methods in enhancing the signal-to-noise ratio for regional modelling, and of course the benefits of using a long time series of time-variable gravimetry to examine the long-term mass flux over glaciated areas. As this kind of data, e.g. from the GRAIL mission orbiting the moon, or from GRACE follow-on missions, continue to evolve as technology improves, so have the methods to study them. Pushing the envelope of the analysis will ensure that satellite gravity, even when other, more direct observations, should be lacking, will continue to play a major role in studying terrestrial, lunar and planetary systems in the future.

References and Notes

1. J. L. Chen, C. R. Wilson, B. D. Tapley, *Science* **313**, 1958 (2006).

2. S. B. Luthcke, *et al.*, *Geophys. Res. Lett.* **33**, 1 (2006).

3. I. Velicogna, J. Wahr, *Nature* **443**, 329 (2006).

4. J. L. Chen, C. R. Wilson, B. D. Tapley, *J. Geophys. Res.* **116**, 1 (2011).

5. E. J. O. Schrama, B. Wouters, *J. Geophys. Res.* **116**, 1 (2011).

6. W. Krabill, *et al.*, *Science* **289**, 428 (2000).

7. W. Krabill, *et al.*, *Geophys. Res. Lett.* **31**, 1 (2004).

8. H. J. Zwally, *et al.*, *Journal of Glaciology* **51**, 509 (2005).

9. E. Rignot, P. Kanagaratnam, *Science* **311**, 986 (2006).

10. R. Thomas, E. Frederick, W. Krabill, S. Manizade, C. Martin, *Geophys. Res. Lett.* **33**, 1 (2006).

11. E. Rignot, J. E. Box, E. Burgess, E. Hanna, *Geophys. Res. Lett.* **35**, 1 (2008).

12. M. van den Broeke, *et al.*, *Science* **326**, 984 (2009).

13. I. Joughin, W. Abdalati, M. Fahnestock, *Nature* **432**, 608 (2004).

14. A. Luckman, T. Murray, *Geophys. Res. Lett.* **32**, 1 (2005).

15. A. Luckman, T. Murray, R. de Lange, E. Hanna, *Geophys. Res. Lett.* **33**, 1 (2006).

16. I. M. Howat, I. Joughin, T. A. Scambos, *Science* **315** (2007).

17. I. Joughin, *et al.*, *Science* **320**, 781 (2008).

18. G. Ramillien, *et al.*, *Global and Planetary Change* **53**, 198 (2006).

19. B. Wouters, D. Chambers, E. J. O. Schrama, *Geophys. Res. Lett.* **35**, 1 (2008).

20. I. Velicogna, *Geophys. Res. Lett.* **36**, 1 (2009).

21. S. Swenson, J. Wahr, *Geophys. Res. Lett.* **33**, 1 (2006).

22. S. A. Kahn, J. Wahr, M. Bevis, I. Velicogna, E. Kendrick, *Geophys. Res. Lett.* **37**, 1 (2010).

23. F. J. Simons, F. A. Dahlen, M. A. Wieczorek, *SIAM Review* **48**, 504 (2006).

24. F. J. Simons, F. A. Dahlen, *Geophys. J. Int.* **166**, 1039 (2006).

25. S. Swenson, J. Wahr, P. C. D. Milly, *Water Resources Research* **39**, 1 (2003).

26. D. Slepian, *SIAM Review* **25**, 379 (1983).

27. M. Cheng, B. D. Tapley, *J. Geophys. Res.* **109**, 1 (2004).

28. J. Wahr, M. Molenaar, F. Bryan, *J. Geophys. Res.* **103**, 30205 (1998).

29. A. Paulson, S. Zhong, J. Wahr, *Geophys. J. Int.* **171**, 497 (2007).

30. An estimate of uncertainty in the post-glacial rebound model could be added to this trend uncertainty if so desired.

31. January 2011 is a missing data month, so our estimated signal is interpolated for January 15th, 2011 and this value is used.

32. O. M. Johannessen, K. Khvorostovsky, M. W. Miles, L. P. Bobylev, *Science* **310**, 1013 (2005).

33. T. Murray, *et al.*, *J. Geophys. Res.* **115**, 1 (2010).

34. This work was supported by the National Science Foundation, grant EAR-EAR-1014606 to F. J. S. We thank Kevin W. Lewis, Allan M. Rubin, and Walter Szeliga for helpful discussions.

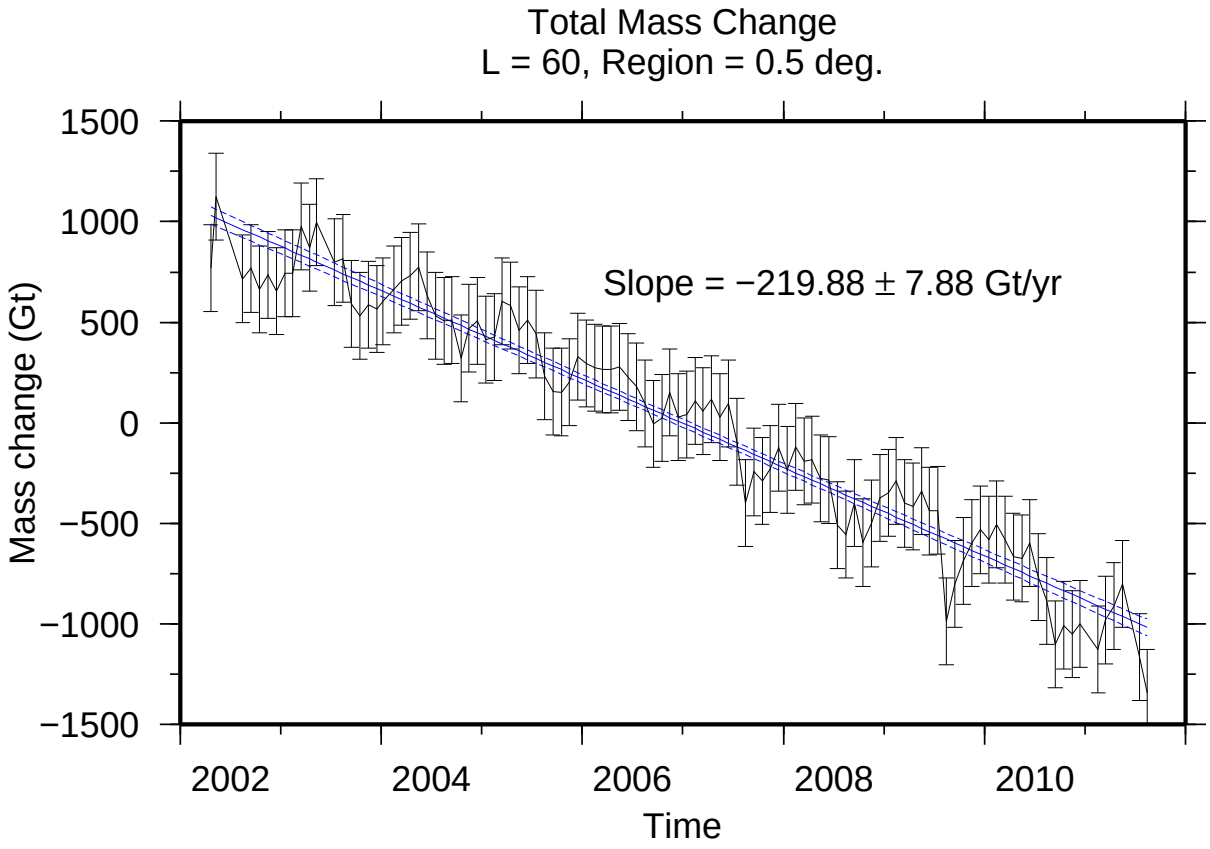

Figure 1: Total mass change trend for Greenland. The solid black line is the raw GRACE monthly solution projected into the Slepian basis optimized to capture the interior of the coastlines of Greenland plus a 0.5° buffer region, and a bandwidth of $L = 60$. The solid blue line is the best-fitting linear trend. The dashed blue lines represent the two-sigma error envelope of this fit.

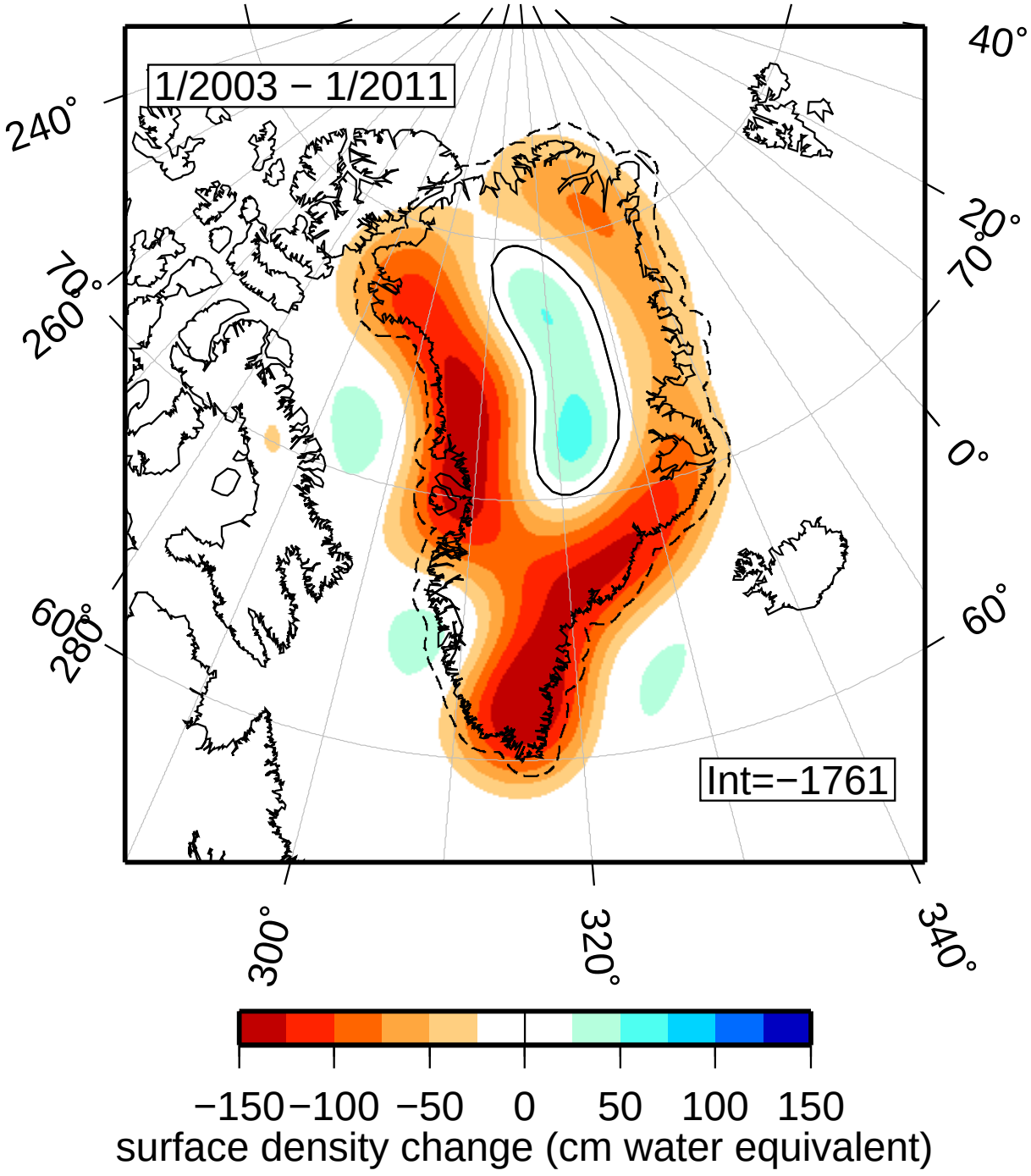

Figure 2: Geographical pattern of the mass change over Greenland averaged for the period between 1/2003 and 1/2011. The map is the result of the combination of signal estimates conducted on individual time series of Slepian-function expansion coefficients. The integral value "Int" for the entire epoch is shown in Gt/yr. The zero cm water contour shown in black.

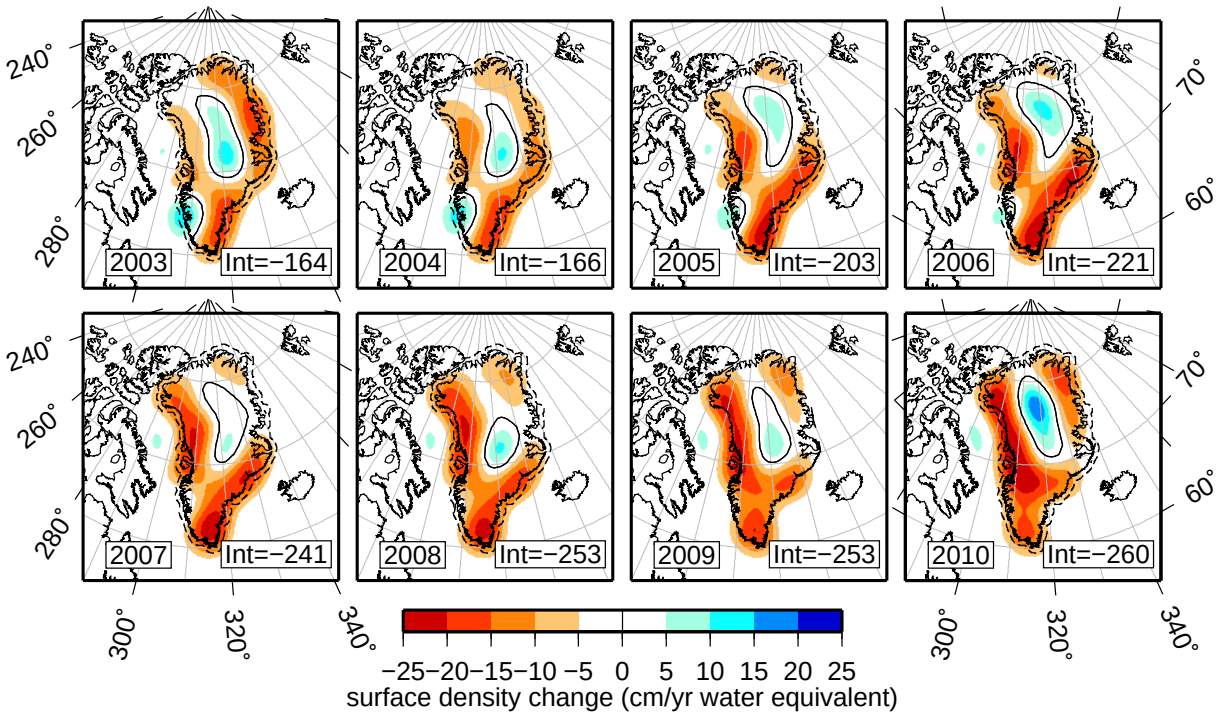

Figure 3: Yearly-resolved maps of mass change over Greenland from 2003 to 2010. The sum of these maps was shown in Fig. 2. Every year shown is the difference of the signal estimated between January of that year and January of the next. The integral values of the mass change per year are shown as "Int", expressed in Gt. The zero cm/yr water contours are shown in black.

PREPRINT — DO NOT DISTRIBUTE

Supporting Online Material (SOM)

Christopher Harig,[1*] Frederik J. Simons[1]

[1]Department of Geosciences, Princeton University,
Guyot Hall, Princeton, NJ 08544, USA

[*]To whom correspondence should be addressed; E-mail: charig@princeton.edu.

March 23, 2012

Determination of Noise

GRACE data are released as spherical-harmonic coefficients along with calibrated errors that represent the diagonal elements of the covariance matrix of the estimated global monthly solutions. It is known that these calibrated errors underestimate the variance in GRACE solutions (*1*), and that monthly solutions are dominated by north-south trending linear "stripe" anomalies (*2*). Thus, many authors choose to estimate their own uncertainty for their modeling (*3*), and attempt to remove estimated noise components (*2*, *4*).

Here, we examine each spherical-harmonic coefficient individually as it varies over time, and find a least-squares estimate of a linear term and a seasonal term with a 365 day period. We consider this fit to be an estimate of the signal contained in the GRACE data, and the residuals form a conservative estimate of the noise. Fig. 1, which examines the coefficients spectrally, shows the results of this procedure. Panel (a) shows a single monthly solution of GRACE data, for February 2010; panel (c) shows the prediction of the signal component for

this month; panel (d) shows the residual after subtracting the signal from the data. Generally, the prediction is dominated by energy in coefficients with degrees less than 30. Meanwhile the residual has some energy at low-degree coefficients, but is mainly comprised of energy in coefficients where the order m (and degree l) is $-30 \gtrsim m \gtrsim 30$. This corresponds to the higher-frequency north-south oriented stripes commonly observed. Finally, panel (b) shows the standard deviations of these residual coefficients over all the months considered. We have made the implicit assumption that the noisy stripes seen in GRACE monthly data are related to the satellite-orbit characteristics specific to each month considered, and therefore these stripes should not have a coherent secular expression over time.

In practice, there is little reason to think that time-variable geopotential signals are best estimated from basis functions that spread their energy over the entire globe. For instance, processes that act in different locations at different times (e.g. monsoons) could easily display competing effects in the same spherical harmonic coefficient. Thus in our determination of noise specifically over Greenland, we estimate signal and noise in the Slepian basis to avoid contamination from other regions. However, to illustrate the importance of estimating the noise covariance and accounted for it in the subsequent analysis, the global spherical-harmonic analysis performed here provides a convenient example.

Covariance of the Noise

We use the spherical-harmonic coefficient residuals from each month to construct a covariance matrix (Fig. 2, shown as a correlation matrix). The residual correlation matrix shows many off-diagonal terms with large correlations. This is contrary to what is normally assumed by other authors, who examine only the diagonal elements of this matrix (the variance) and assume the off-diagonal terms are zero.

These large covariance terms make important contributions to the observed spatial covariance on the sphere. In Fig. 3 we show the difference in *spatial* covariance when the full *spectral* covariance matrix, or only the variance (its diagonal elements) are being used. We consider the covariance between a point in central Greenland with all the other points on the Earth, and do the same with a point in western Antarctica.

Additionally, in Fig. 4 we show how our spatial variance compares with the calibrated errors distributed with the monthly geopotential solutions. Most notably, our spatial variance has significant longitudinal dependence compared to the calibrated errors, while also displaying somewhat higher values of standard deviation than the calibrated errors. It is clear that without the use of the full covariance matrix, estimates of the error in mass change results may be inaccurate. By taking a conservative estimate of the full noise covariance of the data into account we can have high confidence in our mass estimates compared to the results derived from techniques that don't.

The spherical Slepian basis

Given that (1) time-variable gravity signals often originate in specific regions of interest, (2) our data are discreetly measured and therefore have a bandlimit, and (3) we may wish to exclude some portion of the spectrum where the error terms are expected to dominate, then we desire an orthogonal basis on the sphere that is both optimally concentrated in our spatial region of interest and bandlimited to a chosen degree. For this purpose we use the spherical analog to the classic Slepian concentration problem (*5–8*), and define a new set of basis functions

$$g_\alpha(\hat{\mathbf{r}}) = \sum_{l=0}^{L} \sum_{m=-l}^{l} g_{\alpha,lm} Y_{lm}(\hat{\mathbf{r}}), \qquad g_{\alpha,lm} = \int_\Omega g_\alpha(\hat{\mathbf{r}}) Y_{lm}(\hat{\mathbf{r}})\, d\Omega. \tag{1}$$

These functions maximize their energy within our region of interest R following

$$\lambda = \frac{\int_R g_\alpha^2(\hat{\mathbf{r}})\, d\Omega}{\int_\Omega g_\alpha^2(\hat{\mathbf{r}})\, d\Omega} = \text{maximum}, \tag{2}$$

where $1 > \lambda > 0$. The Slepian coefficients, $g_{\alpha,lm}$, are found by solving the eigenvalue equation

$$\sum_{l'=0}^{L} \sum_{m'=-l'}^{l'} D_{lm,l'm'} g_{l'm'} = \lambda g_{lm}, \tag{3}$$

where the elements of $D_{lm,l'm'}$ are products of spherical harmonics integrated over the region R,

$$\int_R Y_{lm} Y_{l'm'}\, d\Omega = D_{lm,l'm'}. \tag{4}$$

The Slepian basis is an ideal tool to conduct estimation problems that are linear or quadratic in the data (*8, 9*). The data can now be projected into this basis as

$$d(\hat{\mathbf{r}}) = \sum_{\alpha=1}^{(L+1)^2} d_\alpha g_\alpha(\hat{\mathbf{r}}) = \sum_{l=0}^{L} \sum_{m=-l}^{l} d_{\alpha,lm} Y_{lm}(\hat{\mathbf{r}}) \tag{5}$$

and by using a truncated sum up to the spherical Shannon number,

$$N = (L+1)^2 \frac{A}{4\pi}, \tag{6}$$

where $A/4\pi$ is the fractional area of localization to R, we can sparsely approximate the data, yet with very good reconstruction properties within the region (*10*):

$$d(\hat{\mathbf{r}}) \approx \sum_{\alpha=1}^{N} d_\alpha\, g_\alpha(\hat{\mathbf{r}}) \quad \text{for} \quad \hat{\mathbf{r}} \in R. \tag{7}$$

This procedure is analogous to taking a truncated sum of the Singular-Value Decomposition of an ill-posed inverse problem (*10*). Since the ill-posedness is in part derived from the focus on the limit area of interest, our procedure in effect determines the singular vectors of the inverse problem from the outset, based on purely geometric considerations, which is efficient.

We solve for a Slepian basis for Greenland (Fig. 5) up to the same degree and order of the available GRACE data, thus the bandwidth $L = 60$. We use the coastlines of Greenland and extend them by 0.5° to create the region of concentration R. With truncation at the Shannon

number N the basis has twenty Slepian functions localized to the region, with the twelfth best function (Fig. 5) still concentrated to $\lambda = 86.9\%$.

The Slepian functions are smoothly varying across the land-ocean boundary, and as a result can have reduced sensitivity near this boundary. This is why we extended the concentration region by buffering away from the coastlines. The size of the buffer zone was based on experiments to recover a synthetic mass trend placed uniformly on Greenland's landmass (Fig. 6). In panel (a), we show the results of an experiment where a uniform synthetic signal is placed over Greenland and we attempt to recover this trend. To replicate the experimental conditions faced by the researchers on the ground we add synthetic realizations of the noise generated from our empirical covariance matrix to this synthetic signal. The signal is best recovered when the region of localization is extended away from the coastlines by 0.5°. This buffer region allows us to better measure mass changes near the coastlines of Greenland, but is small enough that we are not influenced by mass changes outside of Greenland, such as in Iceland or Svalbard. In panel (b), we show how the actual recovered mass trends over Greenland vary depending on the bandwidth and buffer (i.e. region) chosen. Roughly the same trend is recoverable for a broad combination of bandwidth and region buffer, however the lower bandwidths will have reduced spatial sensitivity around Greenland.

Analysis in the Slepian basis

We project each monthly GRACE field, which we convert to surface density, into the Slepian basis for Greenland, which results in a time series for each Slepian expansion coefficient. For each of our twenty Slepian coefficients we fit either a 1st, 2nd, or 3rd order polynomial to the time series, in addition to a 365-day period sinusoidal function, depending on whether each additional polynomial term passes an F-test for significance. These quadratic and cubic terms represent the inter-annual changes in the GRACE data over the data time span. Examples of

these fits are shown in Fig. 7. Here we show the time series of some coefficients and their best-fitting functions, where the fitted annual periodic function has been subtracted. Some time series, such as for $\alpha = 20$, are best represented by a higher-order polynomial, while others, such as $\alpha = 11$, are fit by a linear function since higher-order terms do not significantly reduce variance.

The mass change for an average year, shown in Fig. 8, is found by taking the total estimated mass change from 2003–2010 and dividing by time considered. Most of the mass change of this period projects into the first five Slepian functions, however the remaining fifteen functions of the basis are also important to fully capture the spatial pattern of mass change, even if their mass integrals do not form a large part of the total.

After fitting estimated signals in the Slepian domain, the monthly residuals can be used to form an empirical covariance matrix for the Slepian functions (Fig. 2b). This information not only gives us estimates for the uncertainty of the signal estimates for each Slepian function, but it also allows us to determine the overall trend uncertainty for all of Greenland by combining the variance and covariance in error propagation. Using the full covariance information allows us to have high confidence in our trend estimation, more than we feel comfortable with in previous work.

Finally, we can examine the time series for the three most-contributing Slepian functions, which Fig. 9 expresses as the integral of the product of the expansion coefficient and the function. It is clear from this behavior functions that the mass signal trends can be well estimated relative to the variance seen from month to month. The Slepian functions significantly enhance signal-to-noise within the region of interest compared to traditional spherical harmonics, which further validates our approach.

References and Notes

1. M. Horwath, R. Dietrich, *Geophys. Res. Lett.* **33**, 1 (2006).

2. S. Swenson, J. Wahr, *Geophys. Res. Lett.* **33**, 1 (2006).

3. J. Wahr, S. Swenson, I. Velicogna, *Geophys. Res. Lett.* **33**, 1 (2006).

4. J. L. Chen, C. R. Wilson, B. D. Tapley, D. Blankenship, D. Young, *Earth Planet. Sci. Lett.* **266**, 140 (2008).

5. D. Slepian, *SIAM Review* **25**, 379 (1983).

6. M. A. Wieczorek, F. J. Simons, *Geophys. J. Int.* **162**, 655 (2005).

7. F. J. Simons, F. A. Dahlen, M. A. Wieczorek, *SIAM Review* **48**, 504 (2006).

8. F. J. Simons, F. A. Dahlen, *Geophys. J. Int.* **166**, 1039 (2006).

9. F. A. Dahlen, F. J. Simons, *Geophys. J. Int.* **174**, 774 (2008).

10. F. J. Simons, *Handbook of Geomathematics*, W. Freeden, M. Z. Nashed, T. Sonar, eds. (Springer-Verlag, 2010), chap. 30, pp. 891–923.

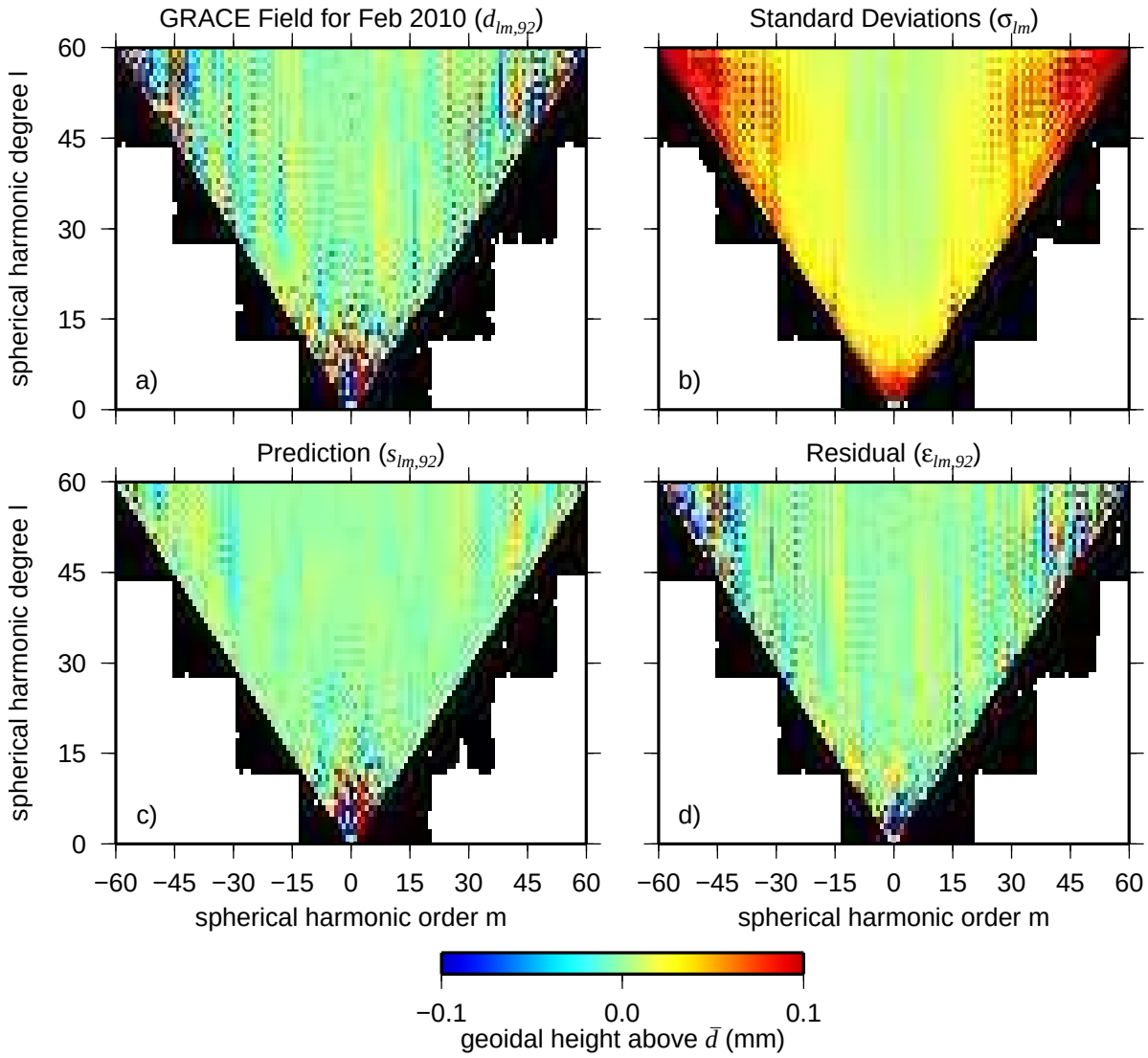

Figure 1: Ordered maps of various spherical harmonic coefficients. (a) The geoidal coefficients ($d_{lm,92}$) of GRACE data from February 2010 after the average of all data months has been removed. (b) Standard deviations ($\sigma_{lm} = [1/M \sum_{n=1}^{M} d_{lm,n}]^{1/2}$ for months $n = 1, ..., M$, where $n = 92$ stands for February 2010) of the residuals as estimated by subtracting the least-squares fits comprising a linear and two seasonal terms with periods 365 and 181 days from each time series of geoidal spherical-harmonic coefficients and computing the covariance of the results. (c) The predicted geoidal coefficients ($s_{lm,92}$) from the least-squares model fit as described before (in panel b). (d) The residual geoidal coefficients ($\epsilon_{lm,92} = d_{lm,92} - s_{lm,92}$) determined by subtracting the predicted coefficients (in panel c) from the GRACE geoidal field (in panel a).

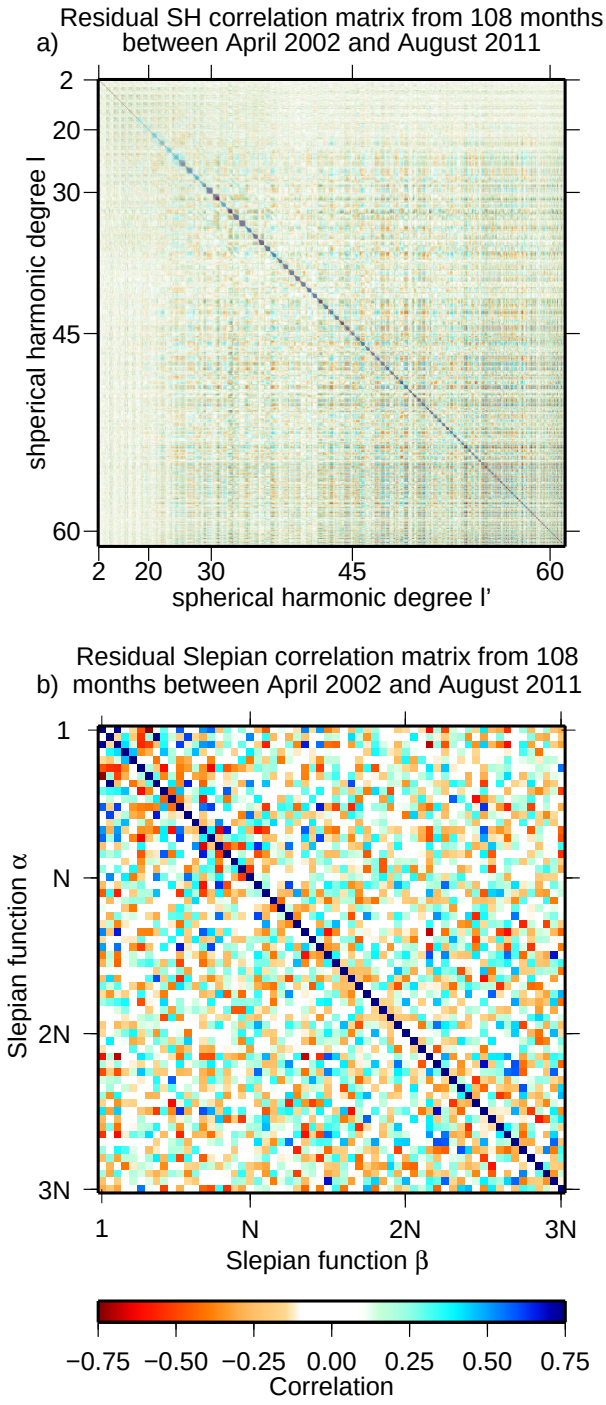

Figure 2: Correlation matrices for spherical-harmonic and Slepian coefficients created from the residuals of 108 months from April 2002 to August 2011. (a) Correlation between spherical harmonic coefficients, derived from the spectral covariance $\mathrm{cov}[\epsilon_{lm}, \epsilon_{l'm'}]$. (b) Correlation between Slepian function coefficients for a basis for Greenland with a region buffer of 0.5° and a bandwidth, $L = 60$. The rounded Shannon number $N = 20$.

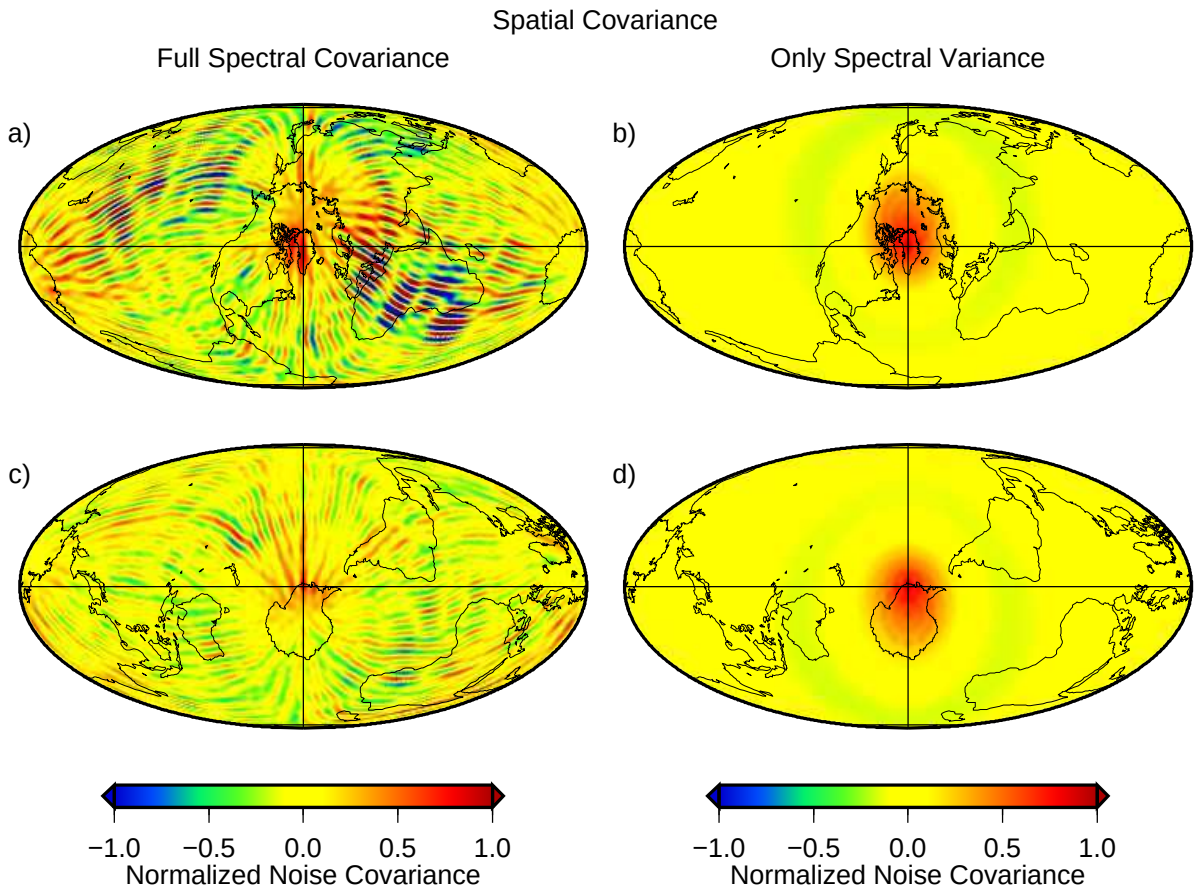

Figure 3: Spatial covariance plots of residuals, $\mathrm{cov}[\epsilon_{\mathbf{r}}, \epsilon_{\mathbf{r}'}]$. Fields have been rotated so that the central cross denotes the point $\mathbf{r}$ with which all the other points $\mathbf{r}'$ covary. In panel (a) and (c) the full spectral covariance matrix is used. Panels (b) and (d) uses only the spectral variance, the diagonal elements of covariance matrix. (a,b) The covariance of a point in Greenland with the rest of the Earth. (c,d) Covariance of a point in western Antarctica with the rest of the globe.

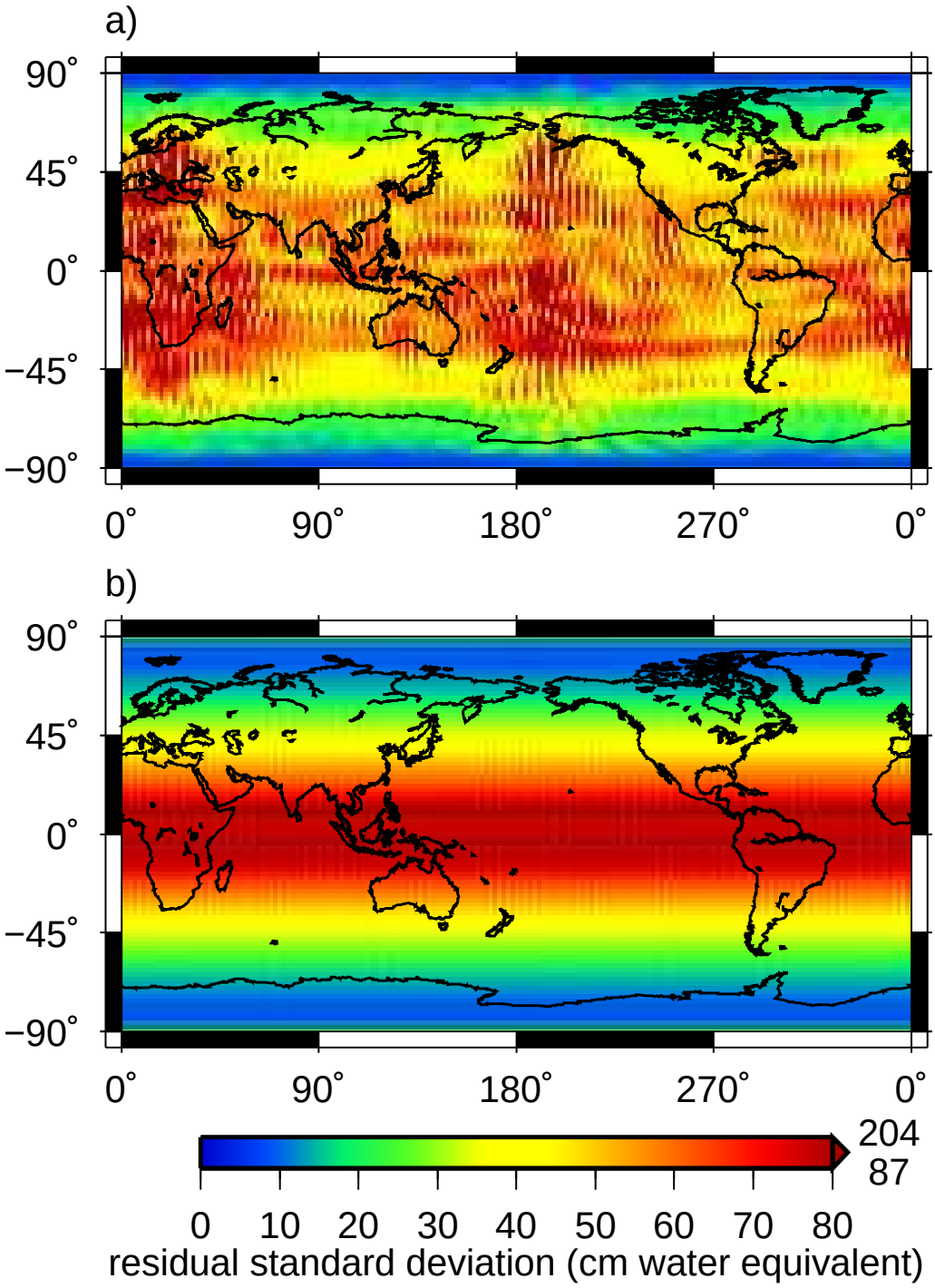

Figure 4: Spatial standard deviation of (a) the diagonal elements of our own estimated covariance matrix and (b) the time-averaged calibrated errors distributed with GRACE monthly solutions. Both plots are saturated at 80 cm water equivalent, but (a) and (b) have the denoted maximums of 204 and 87 cm, respectively.

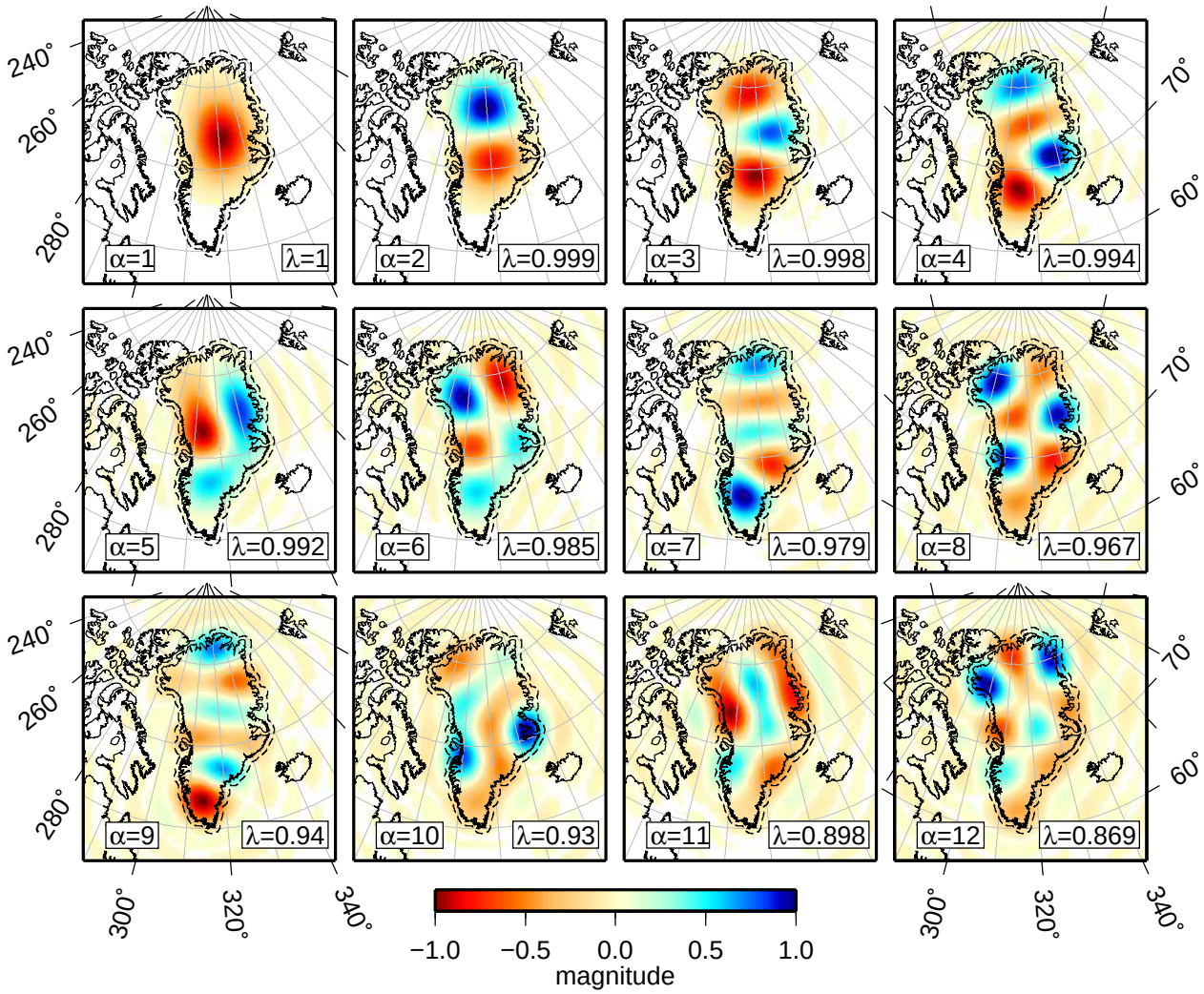

Figure 5: Slepian eigenfunctions $g_1, g_2, ..., g_{12}$ that are optimally concentrated within a region buffering Greenland by 0.5°. Dashed line indicates the region of concentration. Functions are bandlimited to $L = 60$ and are scaled to unit magnitude. The parameter α denotes which eigenfunction is shown. The parameter λ is the corresponding eigenvalue for each function, indicating the amount of concentration. Magnitude values whose absolute values are smaller than 0.01 are left white.

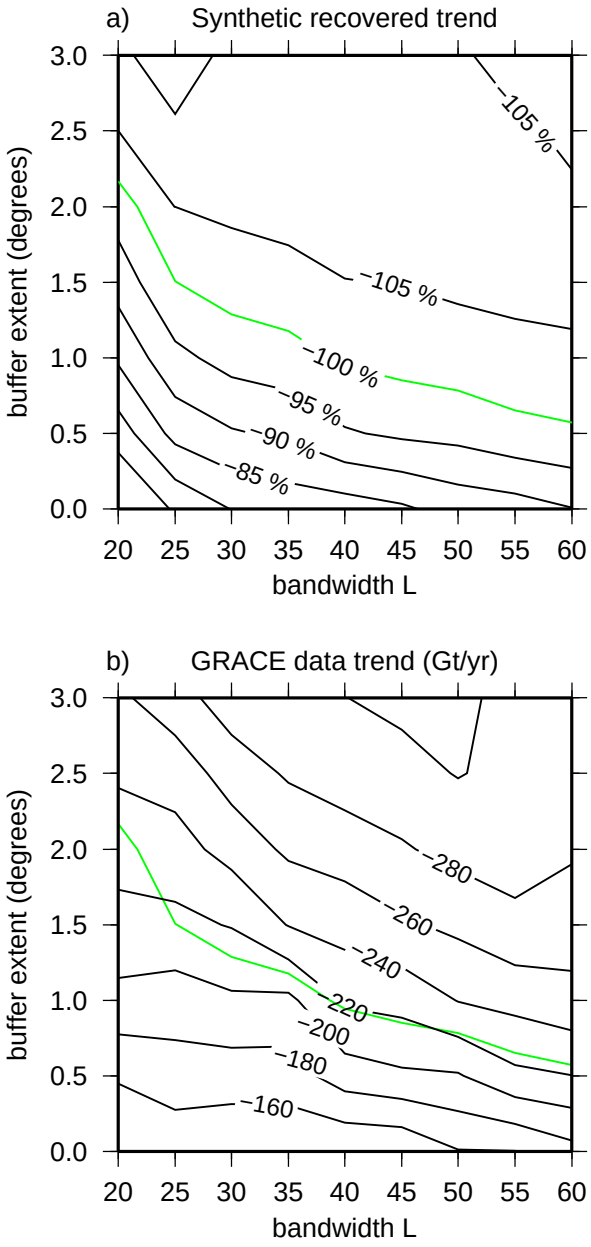

Figure 6: The results of synthetic experiments to examine how recovered trends vary for different bandwidths (L) and different region buffers. (a) We place a uniform mass-loss trend over the landmass of Greenland. To this trend at each month we add a realization of the noise from our residual covariance matrix. We then attempt to recover this trend for different bases over Greenland and report the normalized trend. (b) For the same bases we report the trend recovered from the actual GRACE data in Gt/yr. Also drawn is the 100% recovery contour (from panel a). We use this synthetic experiment to inform our preferred choice of a 0.5° buffer around Greenland.

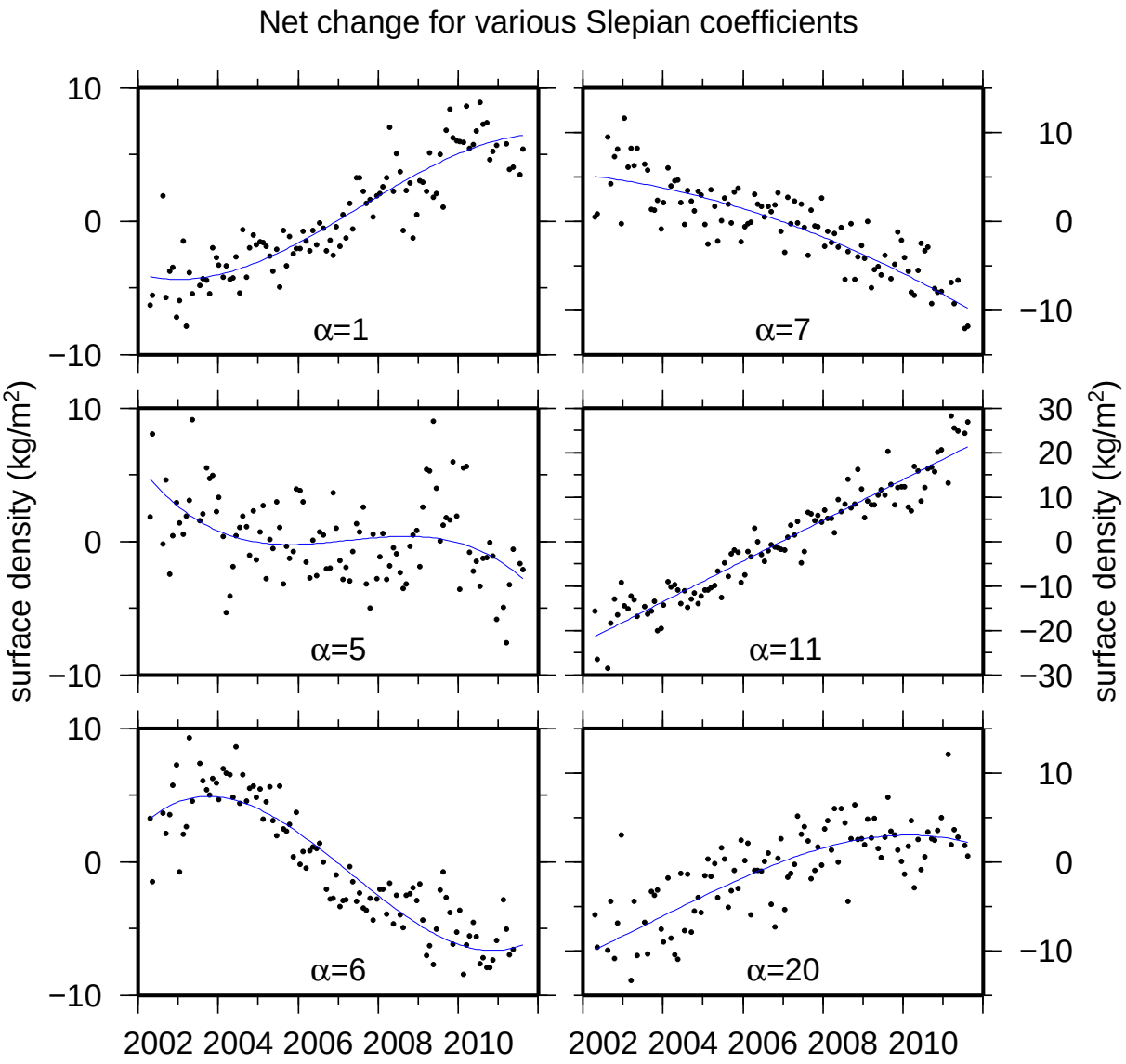

Figure 7: Time series of various (α = 1, 5, 6, 7, 11, 20) Slepian coefficients and their best-fit polynomial (blue lines). Each coefficient is fit by an annual periodic and linear function, as well as quadratic and cubic polynomial terms if those terms pass an F-test for variance reduction. Shown here are the coefficient and fitted function values with the annual periodic function subtracted from both. The mean is removed from each time series.

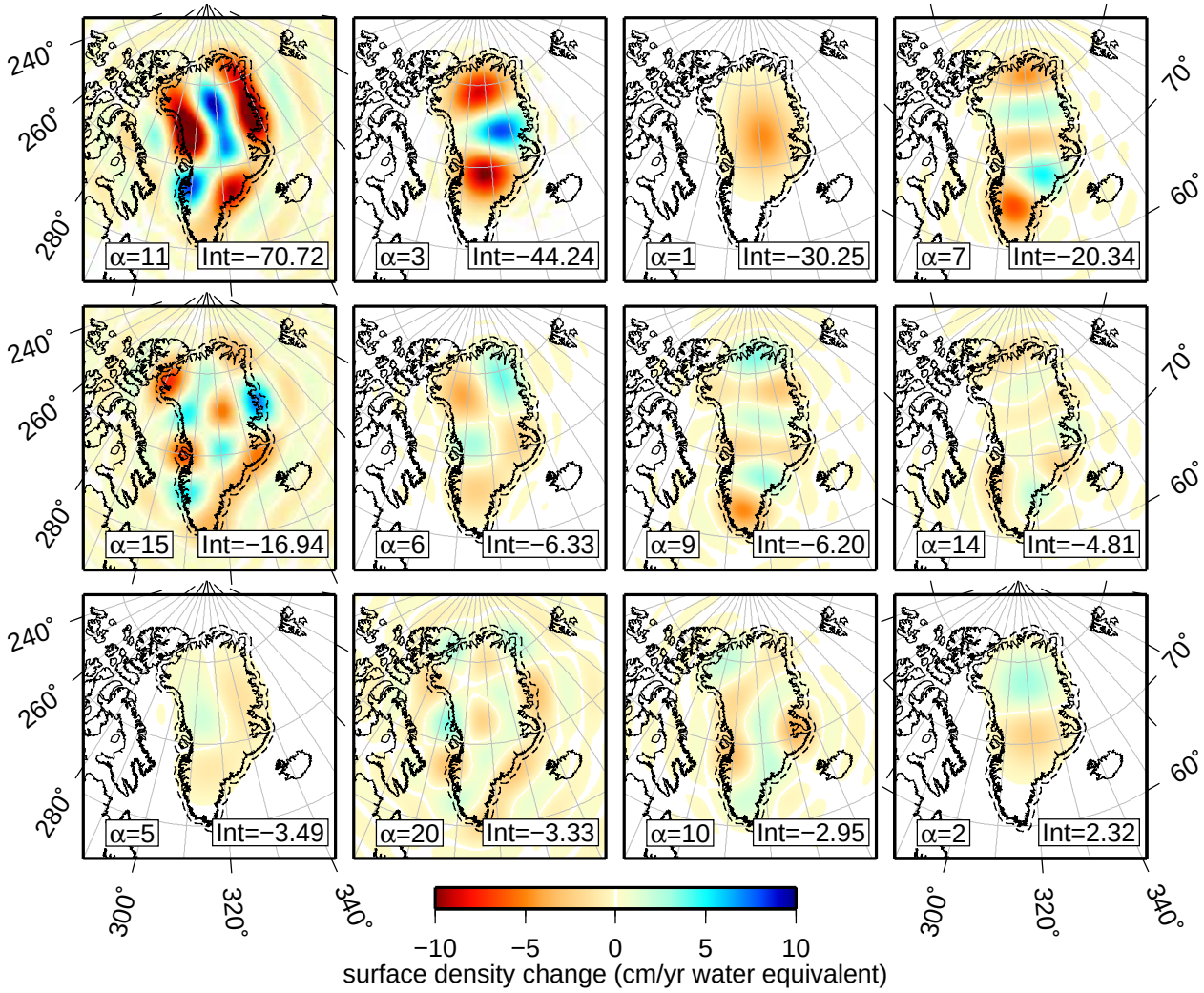

Figure 8: Predicted GRACE annual mass change in the Slepian basis for each of the first twelve eigenfunctions. Each eigenfunction, denoted by its index α, is scaled by the total change in that coefficient from 1/2003–12/2010 divided by the time span (yrs), expressed as the cm/yr water equivalent of surface density. Thus, this represents the mass change for an average year during this time span. The inset variable "Int" displays the integral of each function in the concentration region within the dashed line expressed as the mass change rate of gigatons per year. Surface-density change of absolute value smaller than 0.1 cm/year is left white.

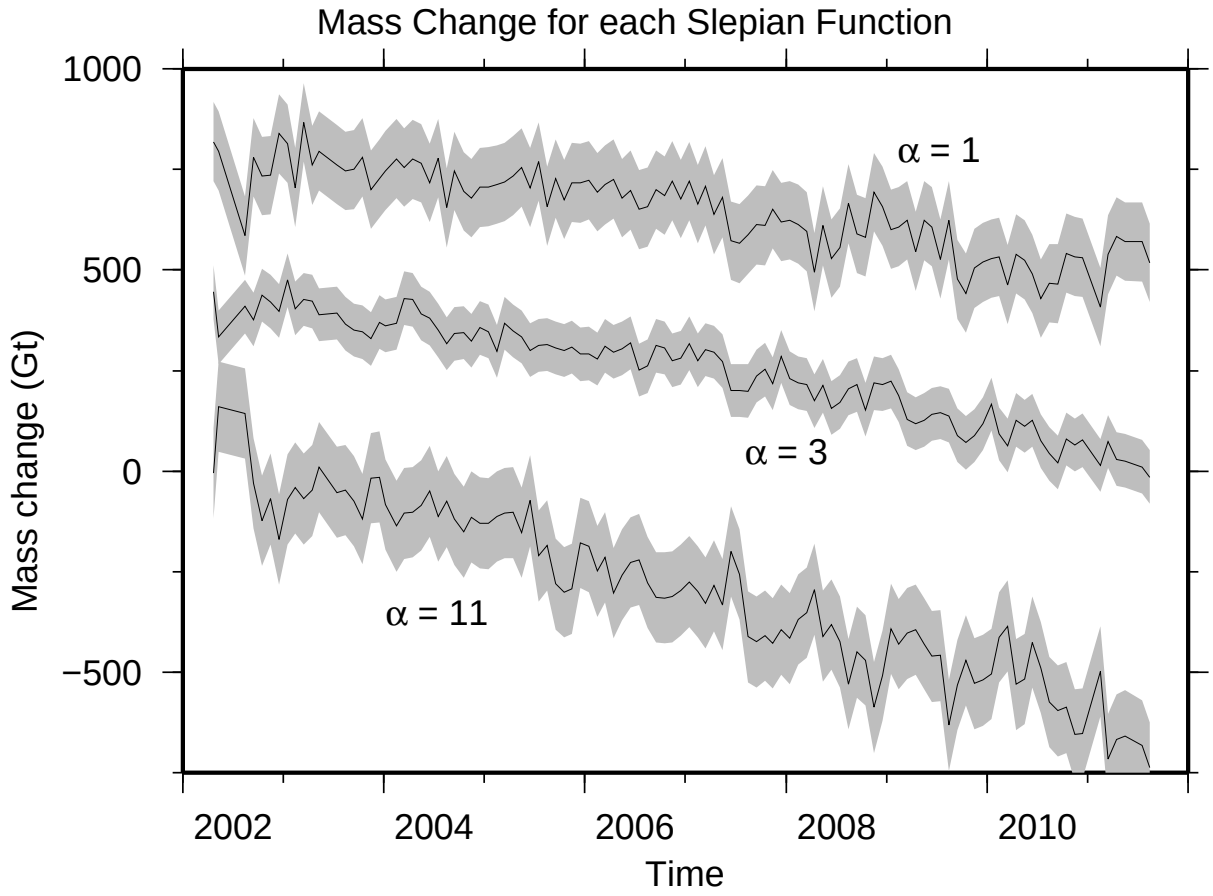

Figure 9: Mass change in gigatons (Gt) for the three most significant Slepian-function terms (α = 1, 3, 11), which contribute more than 70% of total mass change over the data time span. Monthly data are drawn as the solid black lines while the 2σ uncertainty envelopes are drawn in grey. Each function has a mean of zero but has been offset from zero for clarity.